Synthesis and Magnetism of Co_xRh_{1-x} and Co_xRu_{1-x} Nanoparticles

D. Zitoun, C. Amiens, and B. Chaudret*

Laboratoire de Chimie de Coordination - CNRS, 205 Route de Narbonne, 31077 Toulouse Cedex 04, France

M.-C. Fromen, P. Lecante, and M.-J. Casanove

Centre d'Elaboration des Matériaux et d'Etudes Structurales - CNRS, BP 4347, 29 rue Jeanne Marvig, 31055 Toulouse Cedex, France

M. Respaud

Laboratoire de la Physique de la Matière Condensée, INSA, 135 avenue de Rangueil, 31077 Toulouse, France

Received: January 27, 2003; In Final Form: May 7, 2003

The simultaneous decomposition of Co(cyclooctenyl)(COD) (COD: 1,5-cyclooctadiene) and Rh(Acac)(COD) (Acac: acetylacetonate) or Ru(COD)(COT) (COT: 1,3,5-cyclooctatriene) in mild conditions of temperature and pressure leads, in the presence of a polymer (poly(vinylpyrrolidone)), to spherical nanoparticles (NPs), well dispersed and isolated in the organic matrix. All samples display a mean diameter of about 2 nm and a narrow size distribution. Structural investigations by high-resolution electron microscopy (HRTEM) and wide-angle X-ray scattering (WAXS) as well as magnetization measurements by SQUID magnetometry demonstrate the formation of bimetallic alloyed nanoparticles of defined compositions. Cobalt-rich nanocrystals adopt an unusual non periodic polytetrahedral structure while the 4d metal-rich samples display the main features of the bulk structure. More interestingly, the magnetic data evidence a strong enhancement of the magnetic moment per atom compared to bulk values. The coercive field compared to Co monometallic NPs increases strongly with the 4d metal ratio. The alloying with 4d metals is then presented as a precise tool to tune the magnetic properties of nanomagnets and to get softer or harder magnetic materials with high magnetization. The origin of these unusual properties will be discussed in relation with the synthesis conditions and the structure of the NPs.

I. Magnetic Bimetallic Nanoparticles

The synthesis of bimetallic magnetic nanoparticles, the physical properties of which are expected to be highly size-dependent, is currently an important issue for both fundamental[1] and applied research.[2] For instance, the synthesis of ferromagnetic nanoparticles is of great interest for magnetic data storage and in line with the size reduction of microelectronic components. For this application, the magnetic moment and the anisotropy constant of the nanomaterial have to be tuned to increase the superparamagnetic limit well above the room temperature. Since the blocking temperature is a function of the effective anisotropy, one has to achieve the synthesis of nanoparticles of hard magnetic material with controlled size and morphology. This can in principle be achieved by associating a FM metal and a $4d^3$ or $5d^4$ metal. Indeed, if the same tendencies are assumed for nanoparticles and bulk materials, the alloying with noble metals should lead to enhanced anisotropy constant compared to monometallic systems. Thus, one expects that size reduction and the alloying with noble metals will play a cooperative role to get harder magnetic nanomaterials.

From a fundamental point of view, the basic question here concerns the border between a magnetic behavior typical of bulk materials and a small-size material behavior involving predominantly surface effects. Thus, below 3 nm the enhancements of the magnetic moment and anisotropy of the nanoparticles compared to the bulk values are expected. The unusual crystallographic structures which can be induced by the nanometric size and/or elaboration process can reinforce or cancel these effects. In that context, the case of FM 3d/4d alloys (with Rh, Ru, Pd) is particularly interesting since a strong induced polarization can occur on the 4d metal atoms as a consequence of size reduction. Thus, a systematic study is necessary to describe more precisely the phase diagrams and corresponding magnetic properties of nanoparticles.[5]

Several chemical routes have been explored for the preparation of bimetallic materials[6,7] but only few 3d-(4d/5d) magnetic systems have been synthesized so far. For example, the simultaneous decomposition of, on one side iron or cobalt precursors and, on the other, platinum or palladium precursors leads to alloyed FePt,[8] FePd,[9] and CoPt[10] systems, whereas successive decomposition (NiPd[11]) of two monometallic precursors in various proportions, or transmetalation processes (CoPt,[12] CoAg[13]) were reported to generate core−shell bimetallic nanoparticles. The particles are stabilized either by ligands which may control the size of the nanoparticles and lead to nanomaterials containing densely packed nanoparticles or by polymer matrixes which lead to well-dispersed nanoparticles displaying reduced or no magnetic couplings.[8]

Our group has developed an organometallic approach toward the synthesis of metal nanoparticles, whose size, size distribu-

* Author to whom correspondence should be addressed. E-mail: chaudret@lcc-toulouse.fr.

10.1021/jp034215h CCC: $25.00
Published on Web 06/20/2003

tion, and dispersion are all well controlled by the presence in the homogeneous reaction medium of either ligands or organic polymers, generally poly(vinylpyrrolidone) −PVP− (Pt,[14] Ru,[15] and Co[16]). The procedure involves the reaction of a neutral low-valent polyene complex of the desired metal with a reducing gas in mild conditions of pressure and temperature. When the stabilization is achieved by a polymer, the main advantage of this technique regarding the magnetic properties lies in the control of the surface state: no further stabilizing agents are needed and neither the reaction byproducts nor the polymer alter the magnetic properties. In the case of cobalt, nanoparticles have been synthesized, the magnetic properties of which can be compared to the results obtained on clusters from gas-phase experiments.[17,18] In particular, the magnetic moment per atom is enhanced up to 1.94 μ_B for particles of 1.5 ($\pm$0.2) nm diameter. The nanoparticles behave like free clusters, which demonstrates that the dipolar interactions between nanoparticles are negligible. These systems were structurally characterized via high-resolution transmission electron microscopy (HRTEM) and wide-angle X-ray scattering (WAXS) evidencing in the case of cobalt an original polytetrahedral structure.[19]

Using the same chemical route, the synthesis of isolated Pt_xRu_{1-x}[20] and Co_xPt_{1-x}[21] bimetallic nanoparticles, with narrow size distribution and diameters below 3 nm, has been achieved by simultaneous decomposition of two adequate organometallic precursors. In the CoPt system, the influence of the Pt concentration on the anisotropy and magnetic moment of the resulting bimetallic nanoparticles has been demonstrated.

We consider in this paper the synthesis of nanoscale bimetallic CoM (M = Rh, Ru) systems dispersed in an organic polymer matrix. Rhodium and ruthenium are typical examples of 4d metals at the border of FM, which may facilitate their polarization when mixed in one nanoparticle with a 3d FM element. Three Co/M ratios have been studied in both cases: 3/1, 1/1, and 1/3. To our knowledge, the only CoRh nanoparticles reported so far have been obtained by hydrogenation of cobalt and rhodium nitrate salts homogeneously adsorbed on silica supports for applications in catalysis.[22] The only CoRu system has been reported by Schweyer et al.[23] In this case, the nanoparticles were obtained through decomposition of a heterometallic cluster $[NEt_4][Co_3Ru(CO)_{12}]$, once again after its adsorption on silica.

We report hereafter the synthesis of nanoscale Co_3Rh_1, Co_1Rh_1, Co_1Rh_3, and Co_3Ru_1, Co_1Ru_1, Co_1Ru_3 bimetallic systems of very narrow size distribution. In the first part, we present the synthesis of the nanoparticles and the experimental techniques used for their characterization. In a second part, we focus on the structural and magnetic properties. The collected data bring some clear evidence on the bimetallic nature of the nanoparticles and the magnetic data reveal some interesting enhancement of the magnetic moment per atom compared to bulk phases. The alloying of small nanoparticles with Ru or Rh leads to stronger coercive fields compared to the monometallic ones. A preliminary account of this work has been published.[24]

II. Results

The Co_xM_{1-x} (M = Rh or Ru) nanoparticles are obtained from simultaneous decomposition of organometallic precursors ($Co(\eta^3\text{-}C_8H_{13})(\eta^4\text{-}C_8H_{12})$, $Rh(\eta^4\text{-}C_8H_{12})(\eta^2\text{-}C_5H_7O_2)$, and $Ru(\eta^4\text{-}C_8H_{12})(\eta^6\text{-}C_8H_{10})$) in a homogeneous solution, in the presence of a soluble organic polymer (PVP: poly(vinylpyrrolidone) K30) (see Scheme 1). The organometallic precursors have been chosen for their previously evidenced ability to decompose in

SCHEME 1

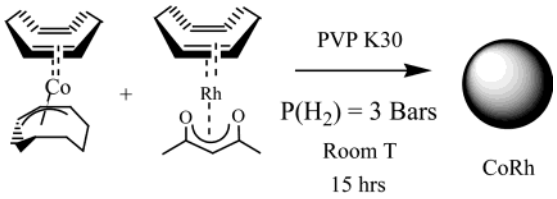

mild conditions of temperature and pressure of dihydrogen (room temperature and P = 3 bar),[14,25] Their decomposition releases only noncontaminating byproducts: cyclooctane is eliminated after evaporation to dryness and does not affect the magnetic properties as observed in the case of monometallic Co particles. The influence of pentane-2,4-diol was not known precisely but one could expect a relatively low surface sensitivity, since an enhancement of magnetism is observed in Co particles exposed to alcohol (methanol), in agreement with free clusters. Finally, the organic polymer and the solvent are chosen to ensure both solubility for each reactant and a good dispersion of the nanoparticles in the matrix, as already published.[26] Up to now, PVP is one of the best ligands which guarantees a very good control of size distribution, with average mean size lower than 3 nm.

The synthesis is performed as follows. The ratio of the precursors is adjusted according to the desired composition of the nanoparticles. The initial dark solution (stable under Ar) is pressurized under dihydrogen in a Fisher−Porter bottle. While the solution is stirred overnight under these conditions, the precursors decompose simultaneously at room temperature. A black precipitate forms and is recovered by filtration. The yield can be improved by performing the precipitation at −80 °C. A further step of dissolution in methanol ensures a good homogeneity of the final material, which is recovered after evaporation of the methanol to dryness. The materials consist of black shiny platelets the chemical microanalyses of which evidence Co/M ratios very close to the initial ratio of the two precursors.

The materials can be manipulated as powders for all structural and magnetic measurements in the solid phase and can be pressed into pellets of any convenient design. The powders can also be redissolved in methanol to form films after deposition of a drop and solvent evaporation, in particular for TEM experiments. To prevent any uncontrolled contamination process of the surface, the powders and the samples dedicated to the structural and magnetic studies are conserved and prepared in a glovebox under Ar.

Structural Study. In all systems, the nanoparticles observed by TEM are well dispersed on the carbon grid with a mean interparticle distance of about 10 nm. Their size distribution is narrow and centered near 2 nm in diameter (see Figure 1). The size distribution is log−normal with a mean size Φ_{mean} and a size dispersion (or polydispersity) σ. All parameters are listed in Tables 1 and 2.

In the high-resolution mode, (HREM), no lattice fringes were observed in particles with a high cobalt content. On the contrary, 4d metal-rich particles exhibit some lattice patterns. For instance, periodicities characteristic of a fcc structure are observed in the Co_1Rh_3 particle displayed in Figure 2 together with its corresponding Fourier transform. Co_1Ru_3 particles display some periodic patterns that could be attributed to a hcp structure, but the even smaller size of these particles prevents any further structural determination. Whatever the system and the composition, the particles display a low contrast and, due to their small dimension, very few fringes can be observed when present. However, as these considerations stand for all the samples, the

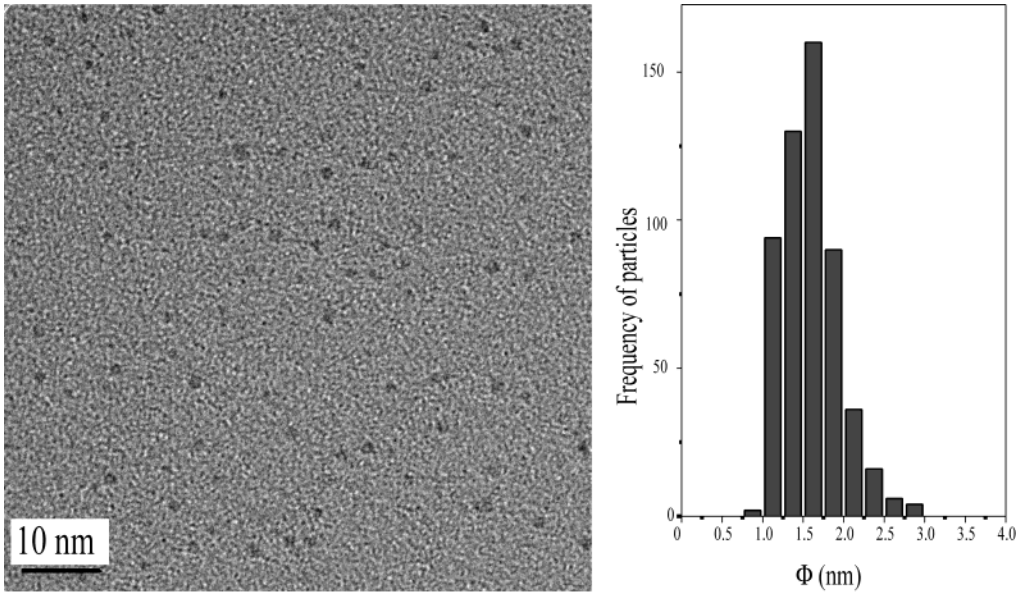

Figure 1. TEM micrograph and size histogram for Co_1Ru_3 particles with a mean size of 1.6 nm.

TABLE 1: TEM, WAXS, and Magnetic Parameters for Co_xRh_{1-x}

parameter	sample				
	Co[13]	Co_3Rh_1	Co_1Rh_1	Co_1Rh_3	Rh[27]
$\Phi_{mean} \pm \sigma$ (nm)	1.5 ± 0.2	1.7 ± 0.3	1.7 ± 0.4	2.3 ± 0.6	1.5 ± 0.3
$L_{coherence}$ (nm)	1.3	1.4	1.5	2.0	1.2
magnetic size (nm)	1.5 ± 0.18	1.6 ± 0.2	1.6 ± 0.2	1.9 ± 0.3	Non FM
average interatomic distance (nm) ($\pm$ 0.0001)	0.2514	0.2629	0.2686	0.2687	0.2696
structure (major)	polytetraedral	polytetraedral	unknown	fcc	fcc

[a] The structure is deduced from HRTEM and WAXS studies and the magnetic size from ZFC/FC fits.

TABLE 2: TEM, WAXS, and Magnetic Parameters for Co_xRu_{1-x}

parameter	sample				
	Co[13]	Co_3Ru_1	Co_1Ru_1	Co_1Ru_3	Ru[10]
$\Phi_{mean} \pm \sigma$ (nm)	1.5 ± 0.2	1.7 ± 0.3	1.6 ± 0.4	1.6 ± 0.3	1.2 ± 0.2
$L_{coherence}$ (nm)	1.3	1.2	1.4	1.3	1.4
magnetic size (nm)	1.5 ± 0.18	1.5 ± 0.2	1.5 ± 0.2	Non FM	Non FM
average interatomic distance (nm) ($\pm$ 0.0001)	0.2514	0.2615	0.2664	0.2694	0.2667
structure (major)	polytetraedral	polytetraedral	unknown	hcp	hcp

[a] The structure is deduced from HRTEM and WAXS studies and the magnetic size from ZFC/FC fits.

presence of lattice fringes in the 4d metal-rich samples only, although sometimes faint, clearly indicate that they present a better crystallographic order.

Evidence of the structural evolution with the composition is better given by the radial distribution functions (RDF) of the interatomic distances obtained from the WAXS measurements. The RDF corresponding to the different specimens are plotted in Figures 3 and 4, the CoRh system and CoRu system, respectively. The RDF obtained for Rh,[27] Ru,[20b] and Co[16] monometallic particles are also included

These plots present a series of peaks, the position and intensity of which are characteristic of the atomic organization inside the particle. The first peak gives the mean metal−metal distance while the position of the last significant peak corresponds to the coherence length, which provides a size estimation of the ordered core of the particle. These different data are reported in Tables 1 and 2.

In all cases, the coherence length is slightly shorter than the mean size determined by TEM. This may be due either to an overestimation in TEM or to the presence of some atomic disorder at the surface of the particle.

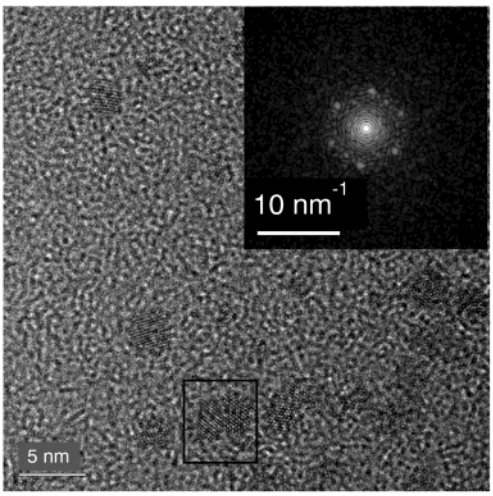

Figure 2. HRTEM micrograph of Co_1Rh_3 particles and Fourier transform of one particle displaying a fcc pattern.

From pure rhodium (respectively, ruthenium) to pure cobalt particles, a gradual decrease of the metal−metal bond length

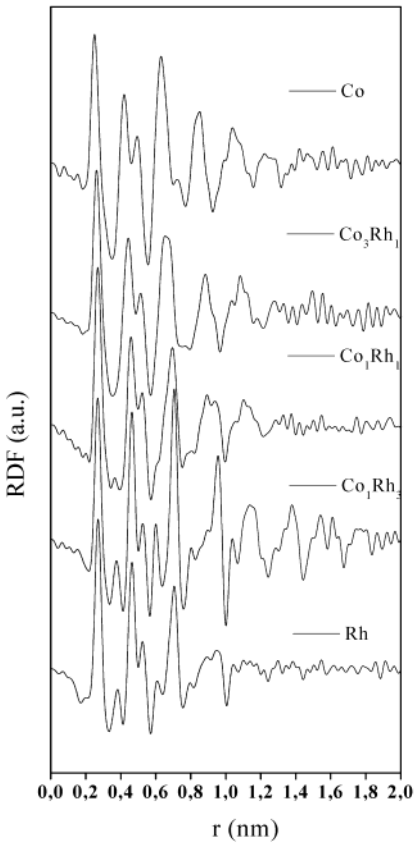

Figure 3. Experimental reduced RDF for different compositions of the Co_xRh_{1-x} system ($0 \leq x \leq 1$).

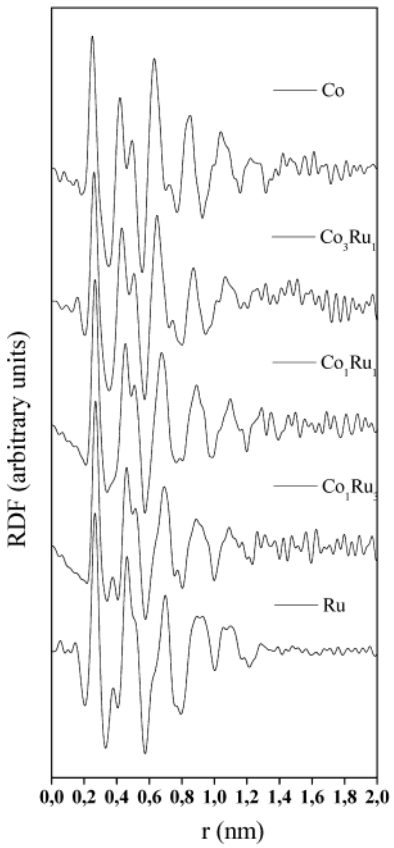

Figure 4. Experimental reduced RDF for different compositions of the Co_xRu_{1-x} system ($0 \leq x \leq 1$).

could be expected as in PtRu particles.[20b] However, as already reported for the CoPt system,[21] the metal−metal bond length very slightly decreases with increasing cobalt content up to the Co_3Rh_1 composition and is strongly contracted from this composition to pure cobalt. A similar behavior is observed in the CoRu system, although it is less pronounced. For a high cobalt ratio, both in CoRh and CoRu systems, the WAXS pattern is almost similar to that found in polytetrahedral cobalt particles,[19] with a dilatation of the interatomic distances. For high Rh or Ru contents, the WAXS patterns display the main features of the pure Rh or Ru particles, i.e., fcc features for Co_1Rh_3 and hcp features for Co_1Ru_3. A comparison between the experimental RDF of Co_1Rh_3 particles and the simulated RDF of a spherical 225-atom fcc Rh cluster is given in Figure 5. The RDF of the intermediate composition Co_1M_1 does not correspond to any known structure.

Magnetic Study. Figure 6 shows a typical zero-field-cooled/field-cooled (ZFC/FC) curve for Co_3Rh_1 nanoparticles, measured in a field of 10 Oe. As a common feature for all samples, the ZFC/FC curves evidence a single sharp maximum on the ZFC curve at a temperature T_B as well as an increasing susceptibility when lowering the temperature on the FC curves. Such behavior is characteristic of superparamagnetism, where T_B corresponds to the blocking temperature. In each case, when lowering the temperature, the FC curve follows the ZFC one and deviates from it at a temperature T_D very close to T_B. The sharpness of the ZFC maximum and the closeness of both T_D and T_B temperatures are representative of the narrowing of the distribution of blocking temperature [$f(T_B)$]. The inverse of the magnetization $M^{-1}(T)$ plotted as a function of the temperature shown in the insets of Figure 6 follows a classical Curie−Weiss law. The dipolar interactions are very low in the system according to the Weiss temperature θ very close to zero ($\theta = 0 \pm 2$ K). The deviation from the Curie behavior observed at high temperature is due to the lowering of the spontaneous magnetization [$M_S(T)$] with increasing temperature. For temperatures above T_B, the magnetization curves as a function of the magnetic field have Langevin form. An hysteresis with nonzero coercive fields and remanant magnetization develops below T_B (see Figures 7 and 8). All these signatures confirm the occurrence of the superparamagnetic transition.

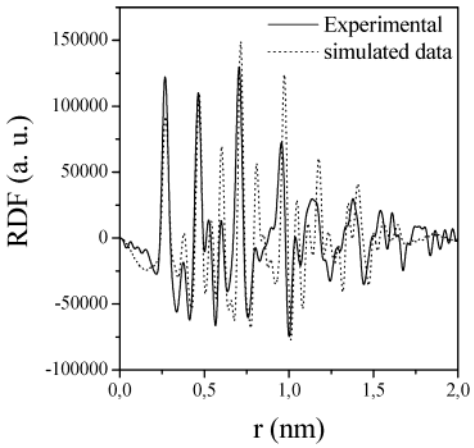

Figure 5. WAXS data of Co_1Rh_3 (solid line) and comparison with the RDF of a perfect 225-atom fcc Rh cluster (dotted line).

Similar behavior has been observed for the different samples; however, with $f(T_B)$, and M_S values representative of each system. Only the $CoRu_3$ system does not display a blocking temperature. As a general tendency, M_S decreases with the introduction of foreign 4d atoms in the Co nanoparticles. This phenomenon is much more sensitive with Ru than with Rh.

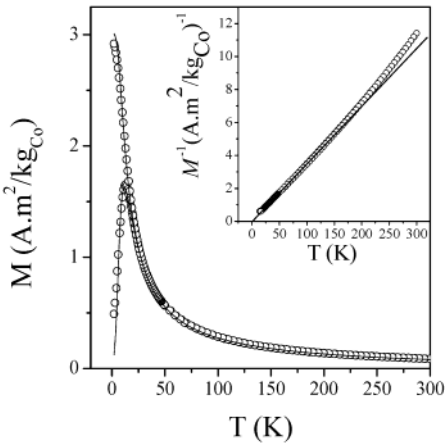

Figure 6. ZFC/FC curve of Co_3Rh_1 at H = 10 Oe (o) and the best fit obtained (____). The inset shows the departure from Curie Law (___) of the inverse ZFC/FC magnetization.

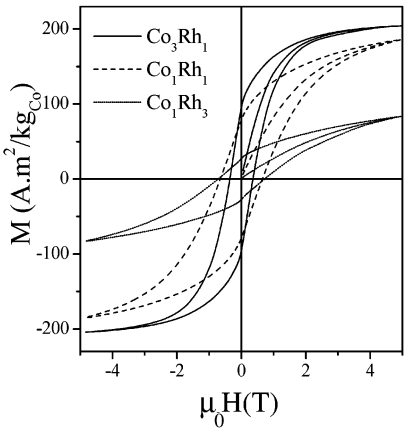

Figure 7. Hysteresis loops of Co_3Rh_1, Co_1Rh_1, and Co_1Rh_3 measured at 2 K with a SQUID magnetometer.

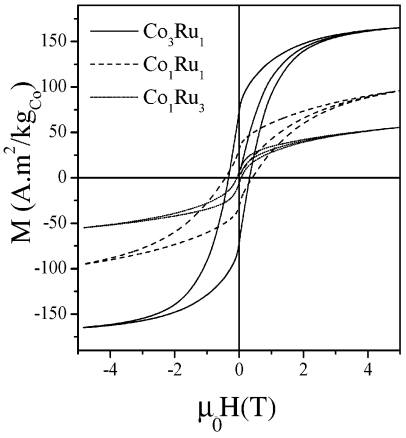

Figure 8. Hysteresis loops of Co_3Ru_1, Co_1Ru_1, and Co_1Ru_3 measured at 2 K with a SQUID magnetometer.

The value of θ close to zero indicates the absence of strong dipolar interactions between the nanoparticles, and thus confirms the regular dispersion of the nanoparticles in the PVP matrix. A volume distribution (log−normal, $f(v)$) was determined upon fitting the magnetic ZFC/FC curves and allowed the determination of a magnetic size (see Tables 1 and 2). These sizes were found in good agreement with the sizes measured on TEM micrographs. Using these size values, the experimental curves, and especially the distribution of blocking temperatures, can be well reproduced without introducing a distribution of anisotropy constants or of spontaneous magnetizations. The distribution of blocking temperatures ($f(T_B)$) can be thus only ascribed to the volume distribution ($f(v)$). Such a behavior confirms that within the different systems of particles presented hereabove, all particles display nearly the same composition. This therefore indicates that the values of K_{eff} and M_S which are determined in these systems reflect the properties of an individual particle of a given size and composition.

TABLE 3: Magnetic Moment Measured at $T = 2$ K and $\mu_0 H = 5$ T and Coercive Fields Extrapolated at 0 K

sample	Co_3Rh_1	Co_1Rh_1	Co_1Rh_3	Co_3Ru_1	Co_1Ru_1	Co_1Ru_3
M(μ_B/at)	1.62	0.95	0.22	1.32	0.5	0.15
$\mu_0 H_C$ (T)	0.50	0.94	1.28	0.50	0.83	0.10[a]

[a] $T = 2$ K, the blocking temperature for Co_1Ru_3, is below 2 K.

The different samples have roughly the same average size between 1.6 and 2.3 nm. They allow the investigation of the intrinsic magnetic properties at a given particle size as a function of the Co content. The formation of bimetallic particles incorporating Co and a non FM metal results in a faster decrease of M_S depending on the metallic composition, also observed by Schweyer et al.[23]

Figures 7 and 8 display the evolution of the hysteresis curves measured at 2 K for the different samples. All these systems display a FM behavior. As a general tendency the magnetization does not saturate even in fields up to 5 T. Increasing the atomic 4d metal concentration considerably affects both the absolute magnetization and the shape of the hysteresis loops. The magnetization loops are irreversible over a large range of magnetic fields, and strong high-field susceptibility is noticeable. Alloying with Rh or Ru induces a reinforcement of the hardness of the material, as indicated by the stronger coercive fields (H_C). However, since H_C is sensitive to the temperature, a more precise estimation of the hardening can be done through the extrapolated values of H_C down to $T = 0$ K, using the expression,

$$H_C(T = 0\ \mathrm{K}) = \frac{H_C(T)}{1 - (T/T_B)^{2/3}}$$

The corresponding values are summarized in Table 3. Alloying with Rh is more effective than with Ru.

From Figures 7 and 8, only the low-field spontaneous magnetization is obtained. Higher fields are necessary to give a precise estimate of the saturation magnetization. However, these measurements are sufficient to extract some general tendencies. The values summarized in Table 3 show the regular decrease of the average magnetic moment per atom with the cobalt content. In all cases, the values are well above the bulk ones, which indicates that probably Co has a stronger magnetic moment and the 4d metal atoms as well. Rh bimetallic systems display the highest magnetizations.

III. Discussion

Since the paper concerns the synthesis of nanoscale alloys, the discussion will focus first on the bimetallic character of the nanoparticles. Here, we have performed the synthesis of magnetic nanoparticles by co-decomposition of two organometallic precursors. As expected, the organometallic approach combined to the use of PVP with low metal concentration allows the control of the growth of the NPs. The TEM studies evidence a regular dispersion of the NPs in the polymer matrix, with narrow size distributions and average diameters smaller than 2

nm. The magnetic properties do not evidence any strong dipolar interaction influence and are representative of well-isolated NPs, in agreement with the TEM pictures.

The concentrations of the two metals in the ensemble of NPs can be simply adjusted through the initial concentration of the two precursors, as confirmed by the chemical analysis. However the determination of the distribution of the atomic species within the population of NPs is not straightforward. Only indirect evidence has been obtained.

The first argument in favor of a regular NP composition can be deduced from kinetic and thermodynamic considerations. The synthesis consists of a simultaneous co-decomposition. Full decomposition of both precursors is done quickly at room temperature. However, in the same conditions (solvent, polymer, and reaction time), full decomposition of Rh(COD)(Acac) alone is only achieved above 70 °C. We hence assume that the decomposition of Rh(COD)(Acac) is catalyzed by a cobalt-based compound, either molecular or colloidal. Therefore, since the decomposition of Rh(COD)(Acac) occurs mostly in a molecular cobalt shell or on a cobalt cluster, the bimetallic nanoparticles have kinetically a higher probability to be formed compared to the monometallic Rh and Co ones. For CoRu samples, the decomposition of both organometallic precursors can be performed at room temperature; nevertheless, the rate of decomposition of Co(cyclooctenyl)(COD) precursor is faster than Ru(COD)(COT) decomposition.

The interpretation of the structural data is also in favor of the hypothesis of bimetallic nanoparticles. Determining the exact crystalline structure is difficult, especially in the case of small particles even in monometallic systems. In general, size reduction promotes unusual high-density packing structures which can be completely different from the bulk ones. Moreover the mild condition of elaboration can lead to original metastable phases. In that context, the case of bimetallic is much more complicated. In the present case, only the structural phases of 4d metal-rich particles have been identified. by HRTEM on suitably oriented NPs. No lattice patterns were observed for other compositions. The WAXS spectra as a function of the Co concentration evidence a progressive transition from the monometallic Co spectrum to the 4d metal ones. The patterns obtained for several data sets coming from different batches of synthesis were found very reproducible. Thus, the fcc (or hcp) phase of pure Rh (or pure Ru) particles transforms progressively into a polytetrahedral-like structure in Co-rich particles. The first metal−metal atomic distance (d_{MM}) remains between the monometallic ones. It should be noticed that the spectra cannot be interpreted using a linear combination of the two monometallic spectra, even if the RDF of Co-rich particles are less resolved than those of 4d metal-rich particles. The peaks at each characteristic distance are sharp enough to consider a single d_{MM}. WAXS studies are therefore in favor of the formation of alloyed rather than core−shell particles.

As a whole, all these data evidence the bimetallic character of the nanoparticles, but they do not permit us to distinguish definitively between a segregated model and a homogeneous alloy. The second hypothesis seems to be more probable considering the elaboration process, the structural data, and magnetic data. Further structural investigations, including element-sensitive ones, are now in progress in order to refine the atomic organization inside the particles. The analysis of the magnetic data also reinforces the hypothesis of bimetallic alloyed particles. For all the bimetallic systems, the spontaneous magnetization plotted versus the temperature decreases, this effect being much more pronounced with increasing 4d metal concentration. Therefore, the Curie temperature is reduced when the Rh or Ru content increases in agreement with a faster decrease of the ferromagnetic correlations. This magnetic behavior is clearly characteristic of an alloy of ferromagnetic and nonferromagnetic elements.

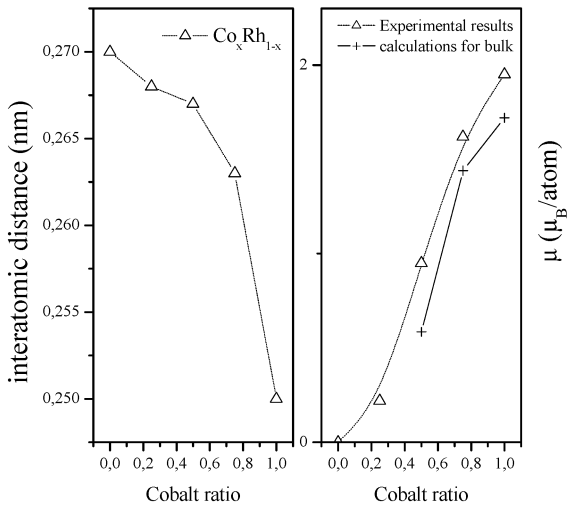

Figure 9. Comparison with bulk Co_xRh_{1-x} (theoretical calculations from Moraïtis et al.[28]) for structural and magnetic data.

The CoRh materials display a hysteresis loop with a coercive field increasing continuously with the Rh content, which further demonstrates the bimetallic character of the system. For the CoRu system, the coercive field similarly increases with the Ru content; however, for a high Ru content (Co_1Ru_3) the blocking temperature cannot be reached and even if the magnetic curve shows an hysteresis, the coercive field cannot be extrapolated to a 0 K value. These results agree with the bimetallic picture of the nanoparticles. They demonstrate that hard magnetic materials can be obtained by alloying with a 4d metal.

Interestingly, these systems display magnetic properties of great interest from a fundamental point of view. The magnetic moment largely exceeds the value of the bulk for all the compositions in CoRh systems (Figure 9). It cannot be attributed to the sole enhancement of the cobalt magnetic moment, even if we assume very small segregated Co particles. The expected high orbital Co contribution cannot explain such a high magnetism. This points toward a large Rh contribution, which may only be reached in nanoscale bimetallic systems. The trend observed for the magnetic moment upon incorporation of rhodium qualitatively resembles that observed in the bulk alloy, even if the magnitude of the effect is much larger in the present case. This trend is in agreement with an alloyed model compared to a segregated one. The CoRu systems reproduce the same tendency, however with lower sensitivity (Figure 10). Thus, ruthenium is not polarized either in small size clusters or in bulk alloys with cobalt. For all these samples, the high values of the magnetic moment evidence the clean surface state of the nanoparticles. The byproducts of the hydrogenation reaction (cyclooctane and pentane-2,4-diol) do not alter the metallic surface, and thus confirms the great advantage of the chosen organometallic precursors.

The enhancement of the magnetization can be well explained qualitatively. Bulk 4d metals do not display any FM behavior. They can become spin polarized by a very small perturbation of the lattice parameter, by alloying with a 3d FM metal[23,24,28] and in "sandwich" Co/M films.[29] Size reduction also induces the appearance of FM as demonstrated by molecular beam

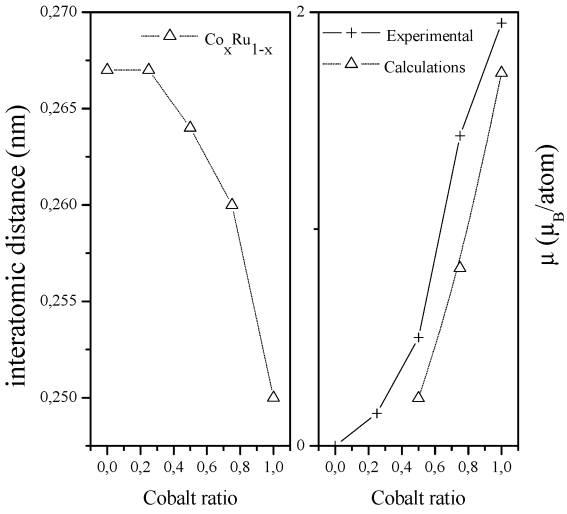

Figure 10. Comparison with bulk Co_xRu_{1-x} (theoretical calculations from Moraïtis et al.[28]) for structural and magnetic data.

deflection measurements for Rh nanoparticles up to 34 atoms,[30] in agreement with theoretical calculations based on tight binding methods.[31] These results demonstrate that size reduction promotes in some cases an electronic polarization in species at the border of FM. For both CoRh and CoRu nanoparticles, the enhancement of the magnetization can be ascribed to the cooperative role of size reduction and 4d metal polarization. The higher electronic polarizability of the Rh compared to the Ru one well explains the stronger magnetism of Rh alloys. Some preliminary X-ray magnetic circular dichroism (XMCD) performed at the ESRF evidence a magnetic moment on Rh, and thus seems to validate these hypotheses.[32]

Conclusion

We describe in this paper the synthesis of Co_xRh_{1-x} and Co_xRu_{1-x} alloys of nanometric size dispersed in a polymer matrix through the simultaneous decomposition of the organometallic precursors in solution in mild conditions. The composition can easily be adjusted according to the initial precursor concentrations. Structural studies allowed us to find some analogies between three CoM systems (M = Ru, Rh, Pt). In particular, for high cobalt contents, an unusual structure is found which is very similar for the three systems and shows similarities to the polytetrahedral phase previously characterized in cobalt nanoparticles. For high M content (Co_1Rh_3, Co_1Ru_3), the crystallographic order is found to be similar to that of the monometallic pure phase (Rh, Ru) with a small change in the lattice parameter. Although both structural and magnetic data favor the formation of alloyed nanoparticles, no definitive proof has been obtained so far. The CoRh system displays a huge enhancement of the magnetic moment per atom compared to bulk value as a result of size reduction and formation of bimetallic particles. The increase in this system of the coercive field compared to that found for Co nanoparticles is also attributed to incorporation of a 4d metal. In the CoRu system, the enhancement is less spectacular but still effective. The quantitative analysis of the polarization induced on Rh and Ru by element-sensitive techniques is currently underway in order to better understand the magnetization process in these nanometric bimetallic systems.

Acknowledgment. The authors thank A. Mari for the magnetization measurements by SQUID, and CNRS for material support. D. Zitoun acknowledges the DGA for a Ph.D. grant and M.-C. Fromen, the French Ministery of National Education and Research, for a Ph.D. grant.

Appendix: Synthesis and Experimental Techniques

Synthesis. All operations were carried out using a standard Schlenk tube or Fisher−Porter bottle techniques under argon.

Materials. PVP was a K30 batch from Aldrich with a molecular weight of roughly 40 000 g mol^{-1}. Carbon monoxide and dihydrogen were from Air Liquide, solvents from SDS.

Sodium was purchased from Fluka. THF was purified just before use by distillation under a dinitrogen atmosphere over sodium and benzophenone. Methanol was purified by distillation over magnesium and kept on a molecular sieve in a glovebox. Pentane was distilled over phosphorus pentaoxide. Solvents were carefully degassed by the freeze−pump−thaw technique before use. The polymers were dried at 80 °C under vacuum in the presence of a phosphorus pentaoxide trap and kept in the glovebox.

The synthesis of Co(η^3-C_8H_{13})(η^4-C_8H_{12}) has been slightly modified from the latest publication. Pyridine (from Fluka) was distilled over potassium hydroxide pellets. Cyloocta-1,5-diene (from Aldrich) was purified through a short alumina column just before use. The solvents were then carefully degassed by the freeze−pump−thaw technique. Cobalt dichloride (purchased from Alfa-Aesar) was kept in a glovebox and dried under vacuum for 2 h before reaction.

Pyridine (16 mL) and cycloocta-1,5-diene (16 mL) were successively added to a carefully degassed suspension of anhydrous cobalt dichloride (4.78 g) in THF. The mixture was kept under stirring for one and a half hours to ensure total complexation of the cobalt, during which the color of the medium turned slightly violet. Sodium (1.69 g) was then added to the mixture which was rapidly cooled to −10 °C in an ethanol bath and was maintained at this temperature under vigorous stirring for 48 h. A black viscous solution was obtained which was further filtered through a glass frit. The black filtrate was evaporated to dryness and the solid was redissolved in 60 mL of pentane. To eliminate residual salts, a second filtration was carried out at −5 °C on the pentane solution. The clear black filtrate was cooled in the freezer at −30 °C, Black crystals formed after one night, were isolated by filtration, and dried under vacuum. Yield 30%.

Microanal. Calcd %: C 69.6, H 9.1. Found %: C 68.96, H 9.67.

The synthesis of Ru(COD)(COT) and Rh(acac)COD have been described in the literature.

CoRh Nanoparticles. *Co_3Rh_1.* Co(η^3-C_8H_{13}) (η^4-C_8H_{12}) (147.1 mg, 0.540 mmol) and Rh(acac)(COD) (55.6 mg, 0.179 mmol) were added in the glovebox in a 350 mL Fisher−Porter bottle. PVP (500 mg) was dissolved at 70 °C in degassed THF (70 mL) and the solution was added to the Fisher−Porter bottle via a cannula. The mixture was stirred, and the bottle was conditioned under 3 bar pressure of dihydrogen. After one night at room temperature under vigorous stirring, the bottle was cooled in an ethanol bath at −80 °C. The nanoparticles embedded in the polymer precipitated and the dark brown solid was dissolved after filtration in degassed methanol (20 mL). The final product was obtained by evaporation as small black pellets.

$$M_{\text{product}} = 310 \text{ mg}$$

Microanalysis:

	mass	atomic
Co	5.0%	76%
Rh	2.8%	24%

Co_1Rh_1. The synthesis is similar to that previously described. Only the stoichiometry was different: Co(η^3-C_8H_{13}) (η^4-C_8H_{12}) (84.2 mg, 0.307 mmol) and Rh(acac)(COD) (95.7 mg, 0.307 mmol).

$$M_{\text{product}} = 320 \text{ mg}$$

Microanalysis:

	mass	atomic
Co	3.1%	49%
Rh	5.6%	51%

Co_1Rh_3. The synthesis is similar to that previously described. Only the stoichiometry was different: Co(η^3-C_8H_{13}) (η^4-C_8H_{12}) (37.3 mg, 0.136 mmol) and Rh(acac)(COD) (126.5 mg, 0.408 mmol).

$$M_{\text{product}} = 310 \text{ mg}$$

Microanalysis:

	mass	atomic
Co	1.5%	25%
Rh	7.7%	75%

CoRu Nanoparticles. *Co_3Ru_1*. Co(η^3-C_8H_{13}) (η^4-C_8H_{12}) (147.1 mg, 0.540 mmol) and Ru(COD)(COT) (56.5 mg, 0.179 mmol) were added in the glovebox in a 350 mL Fisher−Porter bottle. PVP (500 mg) was dissolved in a Schlenk tube in degassed THF (70 mL) at 70 °C, and the solution was added via a cannula to the reactor. The solution was stirred, and the bottle was conditioned under 3 bar pressure of dihydrogen. After one night at room temperature under vigorous stirring, the bottle was cooled in an ethanol bath at −80°C. The nanoparticles embedded in the polymer precipitated and the brown solid was dissolved after filtration in degassed methanol (20 mL). The final product was obtained by evaporation as small black pellets.

$$M_{\text{product}} = 250 \text{ mg}$$

Microanalysis:

	mass	atomic
Co	7.5%	75%
Ru	4.4%	25%

Co_1Ru_1. The synthesis is similar to that previously described. Only the stoichiometry was different: Co(η^3-C_8H_{13}) (η^4-C_8H_{12}) (84.2 mg, 0.307 mmol) and Ru(COD)(COT) (96.1 mg, 0.307 mmol).

$$M_{\text{product}} = 325 \text{ mg}$$

Microanalysis:

	mass	atomic
Co	4.8%	52%
Ru	7.6%	48%

Co_1Ru_3. The synthesis is similar to that previously described. Only the stoichiometry was different: Co(η^3-C_8H_{13}) (η^4-C_8H_{12}) (37.3 mg, 0.136 mmol) and Ru(COD)(COT) (127.7 mg, 0.408 mmol).

$$M_{\text{product}} = 330 \text{ mg}$$

Microanalysis:

	mass	atomic
Co	1.9%	25%
Ru	9.7%	75%

Characterization. Samples were prepared in a glovebox under an argon atmosphere.

Chemical Microanalysis. Analyses were performed at the CNRS center in Vernaison on samples conditioned in sealed tubes under argon.

TEM Experiments. The samples were easily soluble in degassed methanol. Diluted solutions were used to get thin films on carbon-coated copper grid. For a few samples, the contrast was emphasized by the use of carbon grid with micro-holes. At the edge of the holes, the carbon film became thinner and the image quality was enhanced. In the glovebox, TEM samples were prepared by dropping a droplet of the solution on the carbon grid on a filter paper to remove the excess solvent. The carbon grids were stored under inert atmosphere and transferred through air to the microscope. So some oxidation may have occurred during the transfer.

The observations were carried out on a Philips CM30/ST electron microscope operated at 300 kV (with a point resolution of 0.19 nm). The size distribution of the nanoparticles was determined through the numerical analysis of the micro-graphs by counting over about 500 nanoparticles with the software Optimas 6.5.171 (Media Cybernetics, L.P). In this procedure, the different nanoparticles were first identified according to an upper and lower intensity threshold, then counted and measured. High-resolution TEM (HREM) was performed in order to gain structural information on the nanoparticles. The image analysis and Fourier transform were performed with Digital Micrograph 3.0.

WAXS Experiments. Structural characterizations by WAXS were performed in the solid state. The fine powder was introduced in a thin-walled Lindemann capillary of 1.5 mm diameter subsequently sealed under argon. Measurements were performed first on a laboratory diffractometer and then at the ESRF (European Synchrotron Research Facility) on beamline ID15. In the laboratory, measurements of the X-ray intensity scattered by the samples irradiated with graphite-monochromatized molybdenum KR radiation (0.071069 nm) were performed using a dedicated two-axis diffractometer. Time for data collection was typically 20 h for a set of 457 measurements collected at room temperature in the range $0° < \theta < 65°$ for equidistant s values [$s = 4\pi(\sin \theta/\lambda)$]. The data were then integrated. The raw intensity was corrected for contributions generated by other components (polymer, empty capillary) attenuated by sample absorption. The data processing was carried out according to an already published procedure to allow the analysis of the radial distribution function (RDF) of the nanoparticles.[33,34]

Magnetic Measurements. The samples were prepared in gelatin capsules in the glovebox. Magnetic measurements were performed on a SQUID magnetometer (MPMS Quantum Design). The temperature was varied between 2 and 300 K according to a classical zero-field cooling/field cooling (ZFC/FC) procedure in the presence of a very weak applied magnetic field (1 mT), and the hysteresis loops were obtained at different temperatures in a magnetic field varying from +5 to −5 T.

References and Notes

(1) (a) Néel, L *Ann. Geophys.* **1949**, *99*, 5. (b) Jamet, M.; Wernsdorfer, W.; Thirion, C.; Mailly, D.; Dupuis, V.; Melinon, P.; Perez, A. *Phys. Rev. Lett.* **2001**, *86*, 4676.

(2) *Modern Magnetic Materials*; O'Handley, R. C., Ed.; Wiley-Interscience: New York, 1999.
(3) Gallet, J. J; Mariot, J. M.; Journel, L.; Hague, C. F.; Kappler, J. P.; Schmerber, G.; Singh, D. J.; Krill, G.; Goulon, J.; Rogalev, A. *Phys. Rev. B* **1998**, *57*, 7835.
(4) (a) Yu, Y.; Liu, Y.; Moser, A.; Weller, D.; Sellmyer, D. J. *Appl. Phys. Lett.* **1999**, *75*, 3992. (b) Liou, S. H.; Huang, S.; Klimek, E.; Yao, Y. D.; Kirby, R. D. *J. Appl. Phys.* **1999**, *85*, 4334. (c) Carpenter, E. E.; Seip, C. T.; O'Connor, C. J. *J. Appl. Phys.* **1999**, *85*, 5184.
(5) Taniyama, T.; Ohta, E.; Sato, T.; Takeda, M. *Phys. Rev. B* **1997**, *55*, 977.
(6) *Clusters and Colloids. From theory to applications.* Schmid, G., Ed.; VCH: Wienheim, 1994.
(7) (a) Toshima, N.; Yonezawa, T.; *New J. Chem.* **1998**, *22*, 1179. (b) Bönneman, H.; Braun, G.; Brijoux, W.; Bunjmann, R.; Schulze Tilling, A.; Seegovel, K.; Siepen, K. *J. Organomet. Chem.* **1996**, *520*, 143.
(8) Sun, S.; Murray, C. B.; Weller, D.; Folks, L.; Moser, A. *Science* **2000**, *287*, 1989.
(9) Min, C.; Nikles, D. *J. Appl. Phys.* **2002**, *91*, 8477.
(10) Fang, J.; Tung, L. D.; Stokes, K. L.; He, J.; Carun tu, D.; Zhou, W. L.; O'Connor, C. J. *J. Appl. Phys.* **2002**, *91*, 8816.
(11) (a) Teranishi, T.; Miyake, M. *Chem. Mater.* **1999**, *11*, 3414. (b) Hori, H.; Teranishi, T.; Taki, M.; Yamada, S.; Miyake, M.; Yamamoto, Y. *J. Magn. Magn. Mater.* **2001**, *226*, 1910.
(12) Park, J.-I.; Cheon, J. *J. Am. Chem. Soc.* **2001**, *123*, 5743.
(13) Sobal, N. S.; Hilgendorff, M.; Mohwald, H.; Spasova, M.; Radetic, T.; Farle, M.; Giersig, M. *Nano Lett.* **2002**, *2*, 621.
(14) Amiens, C.; De Caro, D.; Chaudret, B.; Bradley, J.; Mazel, R.; Roucau, C. *J. Am. Chem. Soc.* **1993**, *115*, 11638.
(15) Pan, C.; Pelzer, K.; Philippot, K.; Chaudret, B.; Dassenoy, F.; Lecante, P.; Casanove, M. J. *J. Am. Chem. Soc.* **2001**, *123*, 7584.
(16) Osuna, J.; de Caro, D.; Amiens, C.; Chaudret, B.; Snoeck, E.; Respaud, M.; Broto, J.-M.; Fert, A. *J. Phys. Chem.* **1996**, *100* (35), 14571.
(17) Billas, I. M. L; Châtelain, A.; de Heer, W. A. *Science* **1994**, *265*, 1662.
(18) Respaud, M.; Broto, J. M.; Rakoto, H.; Fert, A.; Verelst, M.; Snoeck, E.; Lecante, P.; Mosset, A.; Thomas, L.; Barbara, B.; Osuna, J.; Ould Ely, T.; Amiens, C.; Chaudret, B. *Phys. Rev. B* **1998**, *57*, 1.
(19) Dassenoy, F.; Casanove, M.-J.; Lecante, P.; Snoeck, E.; Mosset, A.; Ould Ely, T.; Amiens, C.; Chaudret, B. *J. Chem. Phys.* **2000**, *112*, 8137.
(20) (a) Pan, C.; Dassenoy, F.; Casanove, M.-J.; Philippot, K.; Amiens, C.; Lecante, P.; Mosset, A.; Chaudret, B. *J. Phys. Chem.* **1999**, *103*, 10098. (b) Dassenoy, F.; Casanove, M.-J.; Lecante, P.; Pan, C.; Philippot, K.; Amiens, C.; Chaudret, B. *Phys. Rev. B* **2001**, *63*, 235407.
(21) Ould Ely, T.; Amiens, C.; Chaudret, B; Dassenoy, F.; Casanove, M.-J.; Lecante, P; Mosset, A.; Respaud, M.; Broto, J. M. *J. Phys. Chem. B* **2000**, *104*, 695.
(22) Kusama, H.; Okabe, K.; Arakawa, H. *Appl. Catal. A* **2001**, *207*, 85.
(23) Schweyer, F.; Braunstein, P.; Estournès, C.; Guille, J.; Kessler, H.; Paillaud, J. L.; Rosé, J. *Chem. Commun.* **2000**, 1271.
(24) Zitoun, D.; Respaud, M.; Fromen, M. C.; Casanove, M. J.; Lecante, P.; Amiens, C.; Chaudret, B. *Phys. Rev. Lett.* **2002**, *89*, 037203.
(25) Choukroun, R.; de Caro, D.; Chaudret, B.; Lecante, P.; Snoeck, E. *New J. Chem.* **2001**, *25*, 525.
(26) (a) Hirai, H. *Makromol. Chem. Suppl.* **1985**, *14*, 55. (b) Ould Ely, T.; Amiens, C.; Chaudret, B.; Snoeck, E.; Verelst, M.; Respaud, M.; Broto, J.-M. *Chem. Mater.* **1999**, *11*, 526. (c) Cordente, N.; Toustou, B.; Collière, V.; Amiens, C.; Chaudret, B.; Verelst, M.; Respaud, M.; Broto, J.-M. C. R. *Acad. Sci. Série IIc* **2001**, *4*, 143. (d) Hess, P. H.; Parker, P. H. *J. Appl. Polym. Sci.* **1966**, *10*, 1915.
(27) Pan, C.; Ramirez, E.; Philippot, K.; Chaudret, B. To be published.
(28) Moraïtis, G.; Dreyssé, H.; Khan, M. A. *Phys. Rev. B* **1996**, *54*, 7140.
(29) Dinia, A.; Zoll, S.; Gester, M.; Stoeffler, D.; Jay, J. P.; Ounadjela, K.; van den Berg, H. A. M.; Rakoto, H. *Eur. Phys. J. B* **1998**, *5*, 203.
(30) Cox, A. J.; Louderback, J. G.; Apsel, S. E.; Bloomfield, L. A. *Phys. Rev. B* **1994**, *49*, 12295.
(31) Villaseñor-Gonzalez, P. V.; Dorantes-Davila, J.; Dreyssé, H.; Pastor, G. M. *Phys. Rev. B* **1997**, *55*, 15084.
(32) Detailed analyses are underway and will be reported in a further article.
(33) Dassenoy, F.; Philippot, K.; Ould Ely, T.; Amiens, C.; Lecante, P.; Snoeck, E.; Mosset, A.; Casanove, M.-J.; Chaudret, B. *New J. Chem.* **1998**, *22*, 703−711.
(34) Lu, G.; Guczi, L. *Stud. Surf. Sci. Catal.* **1994**, *83*, 347.